(3) C. Walling, *J. Am. Chem. Soc.*, **71**, 1930 (1949).
(4) S. Teramachi and Y. Kato, *Macromolecules*, **4**, 54 (1971).
(5) J. R. Runyon, D. E. Barnes, J. F. Rudd, and L. H. Tung, *J. Appl. Polym. Sci.*, **13**, 2359 (1969).
(6) J. E. Adams, "Gel Permeation Chromatography", Marcel Dekker, New York, N.Y., 1971, p 391; *Sep. Sci.*, **6**, 259 (1971).
(7) J. V. Dawkins and M. Hemming, *J. Appl. Polym. Sci.*, **19**, 3107 (1975).
(8) F. M. Mirabella, Jr., et al., *J. Appl. Polym. Sci.*, **19**, 2131 (1975); **20**, 959 (1976).
(9) T. Fujimoto, N. Ozaki, and M. Nagasawa, *J. Polym. Sci., Part A*, **3**, 2259 (1965).
(10) H. Matsuda, K. Yamano, and H. Inagaki, *J. Polym. Sci., Part A-2*, **7**, 609 (1969).
(11) R. Konogsveld and C. A. Tuijnman, *Makromol. Chem.*, **38**, 39, 44 (1960).
(12) V. E. Meyer and G. G. Lowry, *J. Polym. Sci., Part A*, **3**, 2843 (1965).
(13) F. M. Lewis, C. Walling, W. Cummings, Er. Briggs, and F. R. Mayo, *J. Am. Chem. Soc.*, **70**, 1519 (1948).
(14) M. S. Matheson, E. E. Auer, E. B. Bevilacqua, and E. J. Hart, *J. Am. Chem. Soc.*, **73**, 5395, 1700 (1951).
(15) J. P. van Hook and T. V. Tobolsky, *J. Am. Chem. Soc.*, **80**, 779 (1958).

Morphological Studies of Oriented Crystallization of High-Density Polyethylene

Takeji Hashimoto,* Satoshi Ishido,† and Hiromichi Kawai

Department of Polymer Chemistry, Faculty of Engineering, Kyoto University, Kyoto 606, Japan

Andrzej Ziabicki

Institute of Fundamental Technological Research, The Polish Academy of Sciences, Warsaw 00 049, Poland. *Received May 23, 1978*

ABSTRACT: Morphological studies of oriented crystallization of a high-density polyethylene were performed by observing small-angle X-ray (SAXS) and light-scattering (SALS) patterns as well as wide-angle X-ray diffraction patterns (WAXS) as a function of molecular orientation in the amorphous phase (melt draw ratio). These patterns were discussed in terms of the change of nucleation parameters in oriented crystallization with draw ratio: (1) the change in bulk free energy of crystallization, the effect of which is identical for all crystals (the "average effect"), and (2) the change in the kinetic factor H, i.e., the fraction of the chain segments effectively attached to growing nuclei which is different for crystals having different orientation with respect to the orientation axis of the sample (the "specific effect"). The angular dependences of the SALS, SAXS, and WAXS patterns suggested that the specific effect associated with the kinetic factor H is dominant over the average effect for a particular crystallization condition studied in this article.

There is some evidence in the literature that the long spacings measured by small-angle X-ray scattering (SAXS) in polyethylene and other polymers behave with temperature and molecular orientation similarly to the theoretical predictions for the critical cluster (nucleus) thickness, l^*, obtained from the nucleation theory. Peterlin[1] observed an increase of the long spacings with increasing crystallization temperature, T (and reduced undercooling ΔT), an effect resulting from increased critical cluster thickness. Similarly, Kobayashi and Nagasawa[2] observed reduction of the long spacings of oriented crystallized polyethylene films with melt-draw ratio, related to the degree of molecular orientation. The reduction of the long spacing has been correlated to and predicted in terms of a reduction in the critical cluster thickness l^*, due to the average change in the bulk free energy of crystallization Δf.

In this article, we have studied morphology of high-density polyethylene films prepared by oriented crystallization by observing the SAXS, wide-angle X-ray diffraction (WAXS), and small-angle light scattering (SALS) as a function of draw ratio. The results will be interpreted by transmitting the parallelism described above also on the relation between the long spacing and critical cluster thickness l^* for differently oriented crystals. Our primary interest will be focused on the role of orientation dependent "specific" or "kinetic factor" H to be discussed in the following section of this article on the nucleation and growth parameters, and therefore on the resulting morphology of oriented crystallized films.

Table I
Characteristics of the Extruded Films[a]

specimen no.	screw velocity, revolutions/min	take-up velocity, m/min	draw ratio	film thickness, μm
1	20	9.2	20-25	15-25
2	30	9.2	12-13	40 ± 5
3	40	9.2	8-9	55 ± 5
4	40	7.2	6.7	75
5	40	4.1	5	100 ± 10
6	40	4.2	4	130 ± 10

[a] The blow-up ratio = 1, temperature of the extruded melt T = 160 °C.

Experimental Section

Material. A high-density polyethylene with viscosity-average molecular weight 7.8×10^4, melt index 0.82 g/10 min, and density 0.963 g/cm^3 (Novatec ET010, Mitsubishi Chemical Industries,

†On leave from the Polymer Research Laboratory, Mitsubishi Chemical Industries, Inc., Tokyo, at the Mizushima Factory, Mitsubishi Chemical Industries, Inc., 3-10, Ushio Dori, Kurashiki 712, Japan.

0024-9297/78/2211-1210$01.00/0

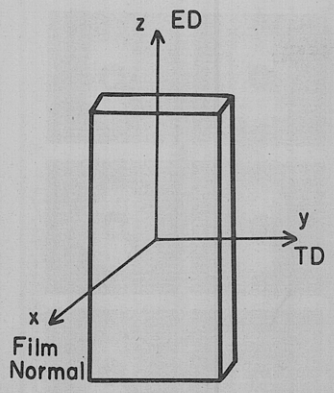

Figure 1. "Through", "edge", and "end" wide-angle X-ray diffraction patterns and small-angle X-ray scattering patterns were taken with the incident beam parallel to the x, y, and z directions, respectively. ED and TD denote extrusion and transverse direction, respectively.

Inc., Tokyo, Japan) was used. The polymer was extruded at 160 °C through a screw extruder with the die of 30 mm in diameter. In Table I are shown extrusion rates, take-up velocities, thickness of the extruded films, and the draw ratios for a series of film specimens used in this study. The draw ratio (in the molten state) was defined as the ratio of the take-up velocity to extrusion velocity. The blow-up ratio defined as the ratio of diameter of the die to that of the extruded films was equal to unity in all specimens.

Methods. Wide-angle X-ray diffraction (WAXS) patterns were obtained at 40 kV and 100 mA, using nickel-filtered Cu Kα radiation. Small-angle X-ray scattering (SAXS) patterns were obtained with nickel-filtered Cu Kα radiation at 40 kV and 100 mA using a rotating anode generator (a Rotaflex RU-100 PL, Rigaku-Denki). The SAXS patterns were taken with a point focussing system under the following collimation conditions: the distances from the first pinhole to the second pinhole, specimen, and photographic film were 250, 310, and 610 mm, respectively; the diameter of the first and second pinhole were 0.5 and 0.2 mm, respectively.

Both WAXS and SAXS patterns were taken with incident X-ray beam directed along three different axes as illustrated schematically in Figure 1; the patterns designated as "through", "edge", and "end" were taken with incident beam directed along x, y, and z axes, respectively. The extrusion direction (ED) for the "through" and "edge" patterns was always vertical.

Long spacings parallel to the ED, denoted as $d_{\parallel}$, and to the transverse direction TD, denoted as d_{+}, were evaluated by measuring the SAXS intensity distributions along the ED and TD by microdensitometric scans of the photographic films and by using Bragg's equation for the scattering angles $2\theta_{max}$ corresponding to maximum intensities.

$$2d \sin \theta_{max} = \lambda \quad (1)$$

where λ is the wavelength of incident X-ray beam.

The crystalline superstructure developed by the oriented crystallization was studied also by measuring depolarized and polarized components of light-scattering patterns with a He–Ne gas laser as an incident beam source (λ_0 = 6328 Å). The H_v and V_v patterns were taken with vertically polarized incident beam and with the analyzer polarized in horizontal and vertical directions, respectively. In all these patterns the ED was vertical.

Results

Both WAXS patterns (Figure 2) and SAXS patterns (Figure 3) show almost identical "through" and "edge" patterns and circularly symmetrical "end" patterns, indicating that orientation of the crystallites and of the lamellar platelets is uniaxially symmetric with ED as the symmetry axis.

The specimen no. 6 obtained with the lowest draw ratio, i.e., with the lowest molecular orientation in the melt, exhibited almost random orientation of the crystallites (Figure 2). With increasing draw ratios, i.e., with increasing molecular orientation, the diffraction arc from the (110) crystal plane has maximum intensity at the equator and that from the (200) crystal plane at the meridan, indicating so-called "a axis" orientation (Figure 2). The WAXS patterns in Figure 2a–c are typical for specimens crystallized at low shear stress as described by Keller and Machin.[3+] Further increase of the draw ratio, and therefore the molecular orientation of the melt, leads to preferential c-axis orientation also described in the Keller–Machin's work and in one of our recent works.[4]

In Figure 3 are shown SAXS patterns of film specimens formed with different draw ratios. The SAXS patterns exhibit single scattering maxima at the scattering angles reciprocally related to the interlamellar spacings. The general trend in the variation of the patterns with increasing draw ratios may be summarized as follows: (i) the meridonal SAXS maximum shifts toward larger scattering angles; (ii) the equatorial SAXS maximum shifts toward smaller scattering angles; (iii) the meridional intensity increases, while the equatorial intensity decreases, leading to a greater angular dependence of the scattering maximum with respect to azimuthal angle. All these features characterize an increase in the anisotropy of SAXS patterns with increasing molecular orientation of the melt.

The first effect (i) is associated with the reduction of the long spacing $d_{\parallel}$ for the lamellae oriented with their normals parallel to ED. The second effect (ii) corresponds to an

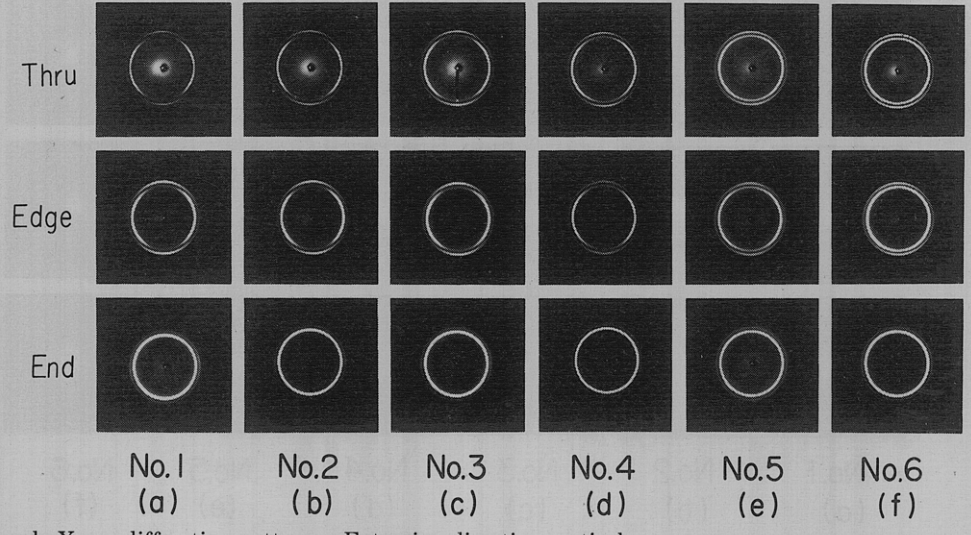

Figure 2. Wide-angle X-ray diffraction patterns. Extrusion direction vertical.

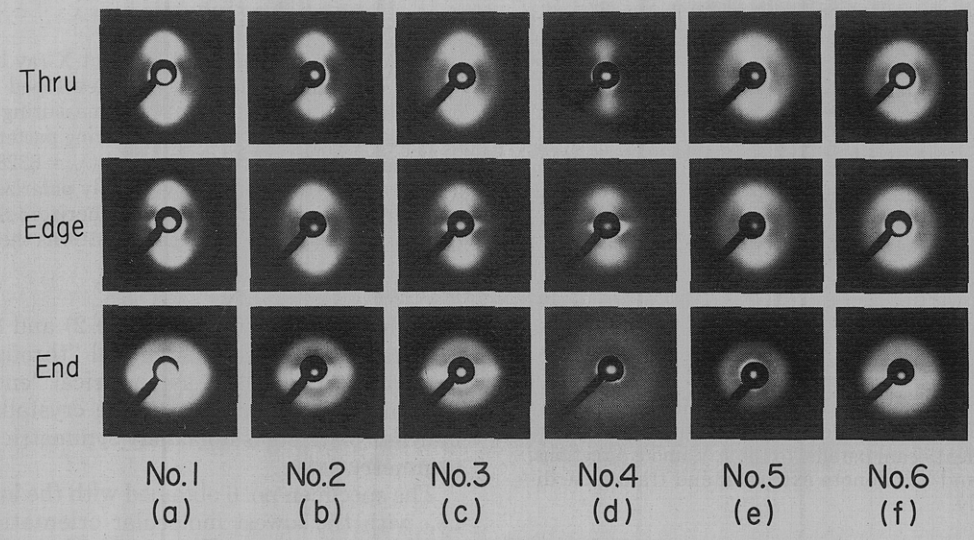

Figure 3. Small-angle X-ray scattering patterns. Extrusion direction vertical.

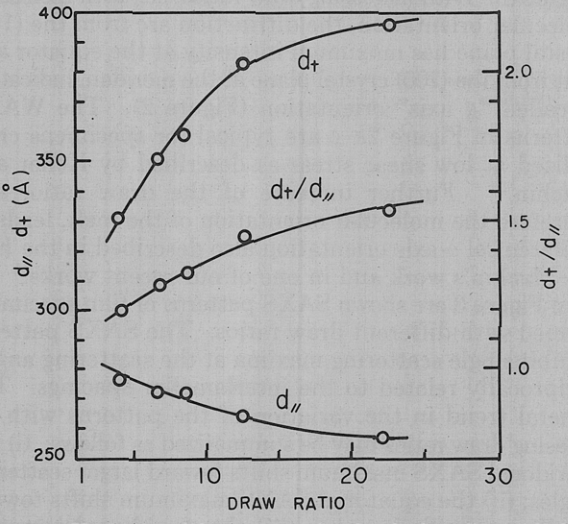

Figure 4. Variation of the long spacing for the lamellae with their normals oriented parallel ($d_{||}$) and perpendicular (d_+) to the extrusion direction and of the ratio $d_+/d_{||}$ with the melt draw ratio.

increase in the long spacing d_+ for the lamellae oriented with their normals perpendicular to ED. The change of the spacing $d_{||}$ and d_+ as a function of the draw ratios is shown in Figure 4. The third effect (iii) indicates that upon increasing the molecular orientation in the melt the lamellar platelets tend to orient with their normals along ED. This observation is consistent with the sharp crystal orientation distributions as found in the WAXS patterns.

The angular dependence of the long spacing is qualitatively considered to arise from that of the lamellar thickness rather than from that of the interlamellar amorphous layer. The angular dependence of the lamellar thickness, in turn, can be explained in terms of the nucleation parameters to be discussed in the following section of this article.

Figure 6 shows effects of the molelcular orientation in the melt upon the higher order superstructure as observed by small-angle light scattering (SALS). The SALS patterns shown in Figure 5e,f obtained from the film specimens crystallized under the lowest draw ratio (no. 2 and 1) are almost identical to typical spherulitic patterns.[5] The H_v patterns are slightly oriented along the meridian, indicating that the internal structure consists of either flattened spherulites with major axes oriented perpendicular to ED, as proposed by Baranov et al.[6] (see Figure (c), or oriented sheaf-like elements with major axes oriented perpendicularly to the drawing axis, as suggested by Hashimoto et al.[7] (see Figure 7b). It is not important for the present study which of these two models is more probable. It is more important to note that in either case the growth rate is larger in the transverse direction than in the extrusion direction.

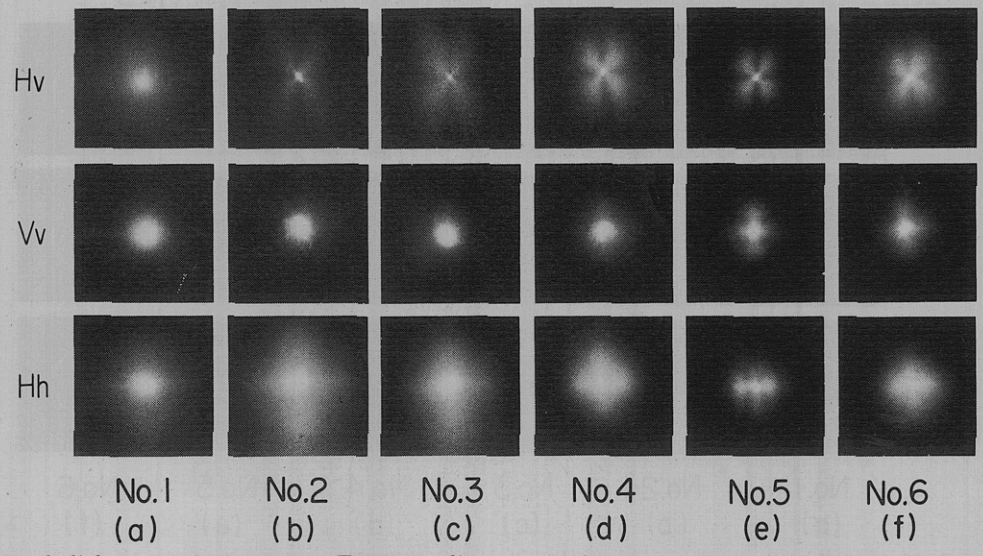

Figure 5. Small-angle light-scattering patterns. Extrusion direction vertical.

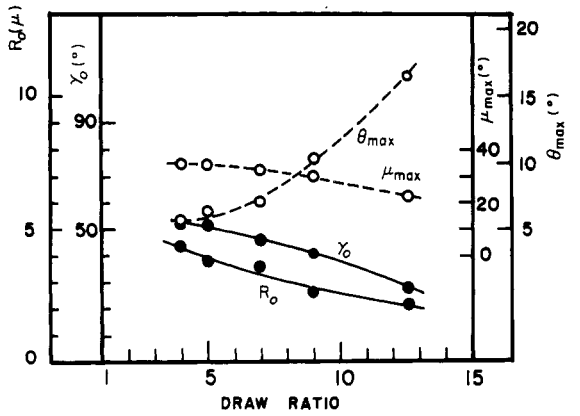

Figure 6. Variation of the angles θ_{max} and μ_{max} and the parameters R_0 and γ_0 with the melt draw ratio.

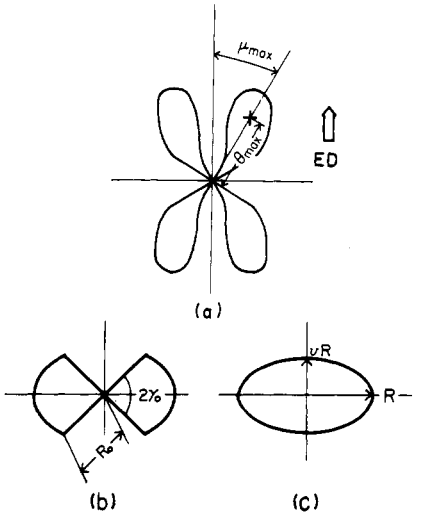

Figure 7. (a) Schematic representation of the H_v pattern and definition of the angles θ_{max} and μ_{max} corresponding to the maximum intensity. (b) and (c) are the models of the superstructure corresponding to the H_v pattern.

The H_v patterns depend on the anisotropy and orientation fluctuations, while the V_v and H_h patterns depend also on the density fluctuations.[5,8] The difference between the V_v and H_h patterns indicates that the fluctuations of anisotropy and orientation are the dominant factors which control the SALS patterns.

With increasing draw ratios, the H_v patterns orient more along the ED, resulting in the butterfly type appearance.[7,9] The scattering angle θ_{max} increases and the azimuthal angle μ_{max} decreases with increasing draw ratios (see Figure 7a). Figure 6 shows the change of θ_{max} and μ_{max} with the draw ratio. Such changes of the H_v patterns correspond to the narrowing of the sheaf (i.e., decreasing γ_0 in Figure 7b) or flattening of the spherulite (i.e., decreasing ν in Figure 7c). For the specimen no. 1 crystallized under the greatest draw ratio, the spherulites or sheaves become very flattened and narrowed, so that the two lobes at $\mu = \pm\mu_{max}$ may overlap and may exist at the angles $\theta = \theta_{max}$ much larger than those for the specimen no. 2.

Theoretical

According to the theory of crystallization developed by one of the present authors,[10,11] the free energy of formation of a crystalline cluster in a liquid or amorphous mother phase, $\Delta\tilde{F}$, which in classical theories was composed of surface free energy and bulk free energy of an isolated cluster, should be completed with another bulk term related to the limited number of single elements (chain segments, kinetic units), H, effectively attached to the cluster[10]

$$\Delta\tilde{F} = \Delta F - (v/v_0)kT \ln H \tag{2}$$

where kT is the Boltzmann free energy, v and v_0 are volumes of the cluster and of the single kinetic element, respectively, and H [$0 \leq H \leq 1$] is the fraction of effective kinetic units, i.e., ones which in an elementary addition time t_0 can be reoriented from their original orientation to the orientation consistent with that of the growing cluster. For a cluster with cylindrical symmetry, radius r, and length (thickness of plate) l, the complete free energy $\Delta\tilde{F}$ assumes the form

$$\Delta\tilde{F} = 2\pi r^2\sigma_e + 2\pi rl\sigma_b + \pi r^2 l[\Delta f - (kT/v_0) \ln H] \tag{3}$$

where σ_e and σ_b denote respectively interface tension in the end and side surfaces of the cluster. $\Delta f = \Delta h(T - T_m^0)/T_m^0$ is the bulk free energy density of cluster formation related to the undercooling ($T_m^0 - T$), Δh is the density of the heat of fusion, and T_m^0 is the equilibrium melting temperature. It should be noted that the value of Δf is negative from its definition.

The critical cluster thickness, l^*, related to the maximum free energy as derived from eq 3

$$l^* = 4\sigma_e/[(kT/v_0) \ln H - \Delta f] \tag{4}$$

and the corresponding maximum value of $\Delta\tilde{F}$ is given by

$$\Delta\tilde{F}^* = 8\pi\sigma_e\sigma_b^2/[(kT/v_0) \ln H - \Delta f]^2 \tag{5}$$

Molecular orientation introduced to the system by deformation or flow, and corresponding to nonuniform distribution of single kinetic elements (chain segments) participating in the growth of a nucleus, can affect nucleation in two ways. First, it affects the bulk free energy of every cluster by reducing entropy[2,12-14] and, to a lesser extent, also the enthalpy[15] of the amorphous phase. The overall effect is an increase of the absolute value of Δf (i.e., an increase of positive value of $-\Delta f$) in eq 3 and, consequently, an increase in the critical nucleation temperature, T_m^0, reduction of the critical thickness, l^*, and the maximum free energy of cluster formation, $\Delta\tilde{F}^*$. Thus molecular orientation leads to higher crystallization temperature, higher nucleation rates, and lower critical thickness of cluster, l^*. This effect, identical for all crystals (consequently designated as *average effect*), is related to the average properties of the amorphous phase. The effect of molecular orientation on the average thermodynamic characteristics of crystallization and on the nucleation kinetics was discussed many years ago by Dunning,[14] Krigbaum and Roe,[13] Kobayashi and Nagasawa,[2,12] and, more recently, by Jarecki.[15]

On the other hand, it can be observed in eq 4 and 5 that an increase of the effectivity parameter H affects nucleation parameters in the same way as decrease (an increase of the absolute value) of the bulk free energy of cluster formation, Δf. The parameter H for bundle-like or irregular (switchboard-type) chain folding depends both on the average molecular orientation of the system (as characterized, e.g., by a molecular elongation ratio λ) and also selectively on the angle between the single kinetic element (segment) and the axis of the growing cluster. This latter effect is different for clusters (and crystals) having different orientations ζ with respect to the orientation axis of the specimen (consequently designated as *specific effect*).

For uniaxial orientation with average molecular elongation λ, the orientation distribution for chain segments $w(\zeta)$ has been derived by Roe and Krigbaum[16] in the form

$$w(\zeta') = (1/4\pi)[1 + (1/2N_s)(\lambda^2 - 1/\lambda)(3\cos^2\zeta' - 1) + ...] \quad (6)$$

where N_s is the number of statistical chain segments in the macromolecule subjected to elongation in the ratio λ. Taking, for deformation ratios λ not too far from unity, only the terms up to the second in the expansion in eq 6 one obtains the average change in the free energy of cluster formation

$$\Delta f = \Delta f(\lambda=1) - (kT/v_0)(1/2N_s)(\lambda^2 + 2/\lambda - 3) \quad (7)$$

and the orientation-dependent kinetic parameter $H(\zeta)$

$$H(\zeta) = 1 - A + (A/10N_s)(\lambda^2 - 1/\lambda)(3\cos^2\zeta - 1) \quad (8)$$

where A is a positive constant related to the mobility of the kinetic units in the crystallizing system[11] and ζ is the angle between the cluster (crystal) axis and the orientation axis in the system, ED.

It can be observed in eq 8 that extension ($\lambda > 1$) corresponds to the highest H values for crystals oriented with their axes parallel to the orientation axis in the system ($\zeta = 0$) and the lowest value at the direction perpendicular to the orientation axis ($\zeta = \pi/2$). The reverse is true for uniaxial compression ($\lambda < 1$). Consequently, one would expect that in polymer systems crystallized in the molecularly oriented state, not only the *average* dimensions l^* and energy $\Delta\tilde{F}^*$ of critical clusters are reduced, but also *differently oriented* crystals are formed from clusters with different critical thickness l^*. These predictions can be summarized as follows:

i. The average critical thickness l^* decreases, and the average nucleation and radial growth rates increase with increasing molecular orientation in the crystallizing system.

ii. The critical thickness l^* and the critical free energy $\Delta\tilde{F}^*$ are reduced by molecular orientation more strongly for crystals oriented along the extension axis ED ($\zeta = 0$) than for crystals oriented perpendicularly ($\zeta = \pi/2$) in the case when the average effect (associated with the term Δf) is dominant over the specific effect (associated with the term H). It should be noted, however, that in the case when the specific effect is dominant over the average effect, l^* and $\Delta\tilde{F}^*$ for crystals oriented at $\zeta = \pi/2$ may increase with molecular orientation contrarily to the characteristics for crystals oriented at $\zeta = 0$.

iii. Higher nucleation rates for crystals oriented along the extension axis (higher values of the parameter H and smaller values of $\Delta\tilde{F}^*$) correspond to crystal orientation distributions sharper than orientation distribution of the original elements (chain segments). This difference is stronger the higher molecular orientation is in the crystallizing system (λ).

Discussion

As discussed in the preceding section, the change of the long spacing $d_{\parallel}$ and d_+ with draw ratio depends on both the average effect of λ on Δf and the kinetic factor H. If the average effect is dominant over the specific effect, both $d_{\parallel}$ and d_+ should decrease with increasing draw ratios; $d_{\parallel}$ being more strongly reduced than d_+ due to the kinetic factor H. The fact that $d_{\parallel}$ decreases while d_+ increases with draw ratios may be interpreted in terms of the dominant contribution of the specific effect over the average effect (see Figure 4).

The tendency of decreasing $d_{\parallel}$ with increasing draw ratios is consistent with that obtained by Kobayashi and Nagasawa.[12] However, the angular dependence of the long spacing cannot be explained in terms of the average effect, but can be interpreted in terms of the specific effect related to the kinetic factor H. The greater azimuthal angle dependence of the SAXS intensity maximum with increasing amorphous orientation can also be explained by an angular dependence of the kinetic factor H.

It should be noted that the strong equatorial streak at the center of some of the end and edge SAXS patterns has nothing to do with the internal structure of the specimens but arises from the total reflection of the incident X-ray beam at the stacked film specimen–air interfaces as described in detail by Hashimoto et al. elsewhere.[17] The total reflection is reduced in the pattern shown in Figure 3 by immersing the specimens into the liquid paraffin which is inert to polyethylene.

The flattening of spherulites or the narrowing of sheaves is a consequence of anisotropy of the growth rate of lamellar crystals, the growth rate being greater along TD than along ED. Although the growth mechanism is not necessarily identical to the nucleation mechanism, we may still expect that the kinetic factor H in the free energy of the cluster formation (eq 2) will also play an important role in the anisotropy of lamellar growth. In other words, similarly to nucleation rate, the growth rate may also be larger for the lamellae having higher effectivity H, i.e., those oriented with their normals parallel to the drawing axis ED. Therefore, the higher the draw ratio is, the higher the molecular orientation is, and the greater the angular dependence of H and thus the greater anisotropy in the growth rate is.

If the superstructure is assumed to be sheaf-like, one can qualitatively estimate the parameters R_0 and γ_0 which characterize the sheaf from the measured angles θ_{max} and μ_{max}, using the method developed by Hashimoto et al.[7] The results are represented in Figure 6. The decreasing value of γ_0 with increasing draw ratio is a consequence of the increased anisotropy in growth rate. The decreasing size of the superstructure with increasing draw ratio is a consequence of the increased nucleation rate and therefore the increased number of nucleating points. The effect may be primarily attributed to the average effect.

Finally it should be noted that the SAXS, WAXS, and SALS patterns are not free from a drawing effect of the structure which has already been crystallized. There should be some minor effects of such "after drawing" on the observed patterns.

Acknowledgment. One of the authors (A.Z.) wishes to express his gratitude to the Japan Society for Promotion of Sciences in Tokyo, which provided him a research grant for a visiting stay in Japan which made possible this joint study.

References and Notes

(1) A. Peterlin in "Man-made Fibers, Science and Technology", Vol. 1, Interscience, New York, N.Y., 1967, p 283.
(2) K. Kobayashi and T. Nagasawa in "Formation of Fibers and Development of Their Structure", Vol. 1, Kagaku Dojin, Kyoto, Japan 1969, p 177.
(3) A. Keller and M. J. Machin, *J. Macromol. Sci., Phys.*, **1(1)**, 14 (1967).
(4) T. Hashimoto, K. Nagatoshi, A. Todo, and H. Kawai, *Polymer*, **17**, 1063 (1976).
(5) R. S. Stein and M. B. Rhodes, *J. Appl. Phys.*, **31**, 1973 (1960).
(6) V. G. Baranov, S. Ya, Frenkel, V. I. Gromov, T. I. Volkov, and R. S. Zurabian, *J. Polym. Sci., Part C*, **38**, 61 (1972).
(7) T. Hashimoto, A. Todo, Y. Murakami, and H. Kawai, *J. Polym. Sci., Polym. Phys. Ed.*, **15**, 501 (1977).
(8) R. S. Stein in "Structure and Properties of Polymer Films", R. W. Lenz and R. S. Stein, Ed., Plenum Press, New York, N.Y., 1973.
(9) T. Hashimoto, A. Todo, and H. Kawai, *Polym. J.*, **10**, 521 (1978).
(10) A. Ziabicki, *J. Chem. Phys.*, **66**, 1638 (1977).

(11) A. Ziabicki, Reports of the Institute of Fundamental Technological Research, Polish Academy of Sciences, No. 60, Warsaw, 1977.
(12) K. Kobayashi and T. Nagasawa, *J. Macromol. Sci., Phys.*, **4**, 331 (1970).
(13) W. R. Krigbaum and R. J. Roe, *J. Polym. Sci., Part A*, **2**, 4391 (1964).
(14) W. J. Dunning, *Trans. Faraday Soc.*, **50**, 1155 (1954).
(15) L. Jarecki, Reports of the Institute of Fundamental Technological Research, Polish Academy of Sciences, No. 26, Warsaw, 1974.
(16) R. J. Roe and W. R. Krigbaum, *J. Appl. Phys.*, **35**, 2215 (1964).
(17) T. Hashimoto, K. Nagatoshi, A. Todo, H. Hasegawa, and H. Kawai, *Macromolecules*, **7**, 364 (1974).

Distortions of Band Shapes in External Reflection Infrared Spectra of Thin Polymer Films on Metal Substrates

D. L. Allara,* A. Baca, and C. A. Pryde

Bell Laboratories, Murray Hill, New Jersey 07974. *Received April 10, 1978*

ABSTRACT: Films of poly(methyl methacrylate), of varying thicknesses from near monolayer to 2 μm, on gold and silicon substrates have been examined by external reflection infrared spectroscopy. The shape of the 1731 cm^{-1} C=O band has been determined as a function of film thickness, angle of incidence, and polarization of the incident beam. Theoretical calculations of the band shape distortions of the C=O stretching mode are in good agreement with the observed spectra. Additional calculations, based on indices of refraction calculated from the Kramers–Kronig relation, demonstrate the effects of wavelength, extinction coefficient, and bandwidth on hypothetical reflection spectra. Some general conclusions are drawn with respect to the types of shifts and distortions one can expect in the reflection spectra of typical organic polymer films. These results suggest that significant care be taken in the assessment of chemical changes from band shifts and splitting in polymer/metal reflection spectra.

I. Introduction

The need often arises, in both fundamental and practical studies, to obtain an infrared spectrum of a thin film on a reflective metal substrate. The use of transmission spectroscopy is effectively precluded by the high absorptivity of the metal. Therefore, spectra must be obtained by internal and/or external reflection techniques (IRS and ERS,[14] respectively). These techniques are not as straightforward experimentally as transmission and problems often arise in quantitative interpretation because reflection spectra may be distorted relative to transmission with significant changes occurring in peak maxima. The physical basis for such distortion involves the significant contribution of the refractive index to the reflectivity of a sample coupled with the rapid changes in the refractive index in the region of an absorption band (the anomalous dispersion). Such effects are of importance, for example, in understanding the chemical and structural nature of thin films by the interpretation of spectral shifts relative to bulk transmission bands. Detailed descriptions of these phenomena, with examples, are given by Harrick[2] for IRS.

Optical effects must also be taken into account in the accurate interpretation of ERS,[2] but few examples quantitatively relating theory and experiment are available. Greenler, Rahn, and Schwartz[1] have experimentally obtained reflection spectra of Cu_2O films on Cu for thicknesses of Cu_2O between 450 and 4200 Å. The 623-cm^{-1} transmission band is shifted to 655 cm^{-1} in the multiple reflection mode with angles of incidence between 84 and 90°. Using theory based on classical physical optics and developed to a great extent in an earlier paper[3] these authors calculated a band shift of 28 cm^{-1} and indicated that further correction of the calculations for small transmission shifts could improve the agreement. However, band splitting predicted by the calculations for 4200 to 12 000 Å films was not observed in the experiments and thus some question remains regarding discrepancies between the experiment and theory over a wide range of thickness for typical experimental conditions. Calculations (but no experiments) were also made for copper surfaces with films of benzene, a weak absorber relative to Cu_2O (extinction coefficient of ~0.07 vs. ~5, respectively). No shifts were predicted from these calculations. Therefore, these authors made the general and potentially useful conclusion that ERS (or RA[14]) spectra of "typical moderately strong infrared bands should be directly comparable with the transmission experiment."

Unfortunately, no other studies are available and some gaps between theory and experiment in ERS still exist. It was of particular importance to us to know whether band distortion effects would arise in organic polymer films (e.g., common metal coating materials) which contained absorbing groups intermediate in extinction coefficients between benzene and Cu_2O and, if so, whether these effects could be exactly calculable from the same theory that was only partially successful for Cu_2O films.[1] For this study, we chose poly(methyl methacrylate) (PMMA), a typical organic material with a distinct C=O stretching band at 1731 cm^{-1}. Films with thicknesses from near monolayer dimensions to 2 μm were prepared on gold substrates and several angles of incidence were used to give typical experimental conditions which spectroscopists might use. In addition, one experiment on a silicon substrate was done to examine the effect of a reflective dielectric material. Using our experimental results as a guide, calculations based on theory were carried out for hypothetical bands at 1000, 1731, and 3000 cm^{-1} to check the effects of variations in index of refraction, extinction coefficient, and wavelength on band distortions. Some useful generalizations are drawn from the experimental and calculated results in the last section. The results and conclusions should be broadly applicable to a variety of organic films and metals because most organic materials have very similar values of refractive indices (near 1.5 in nonab-

0024-9297/78/2211-1215$01.00/0